Asian Journal of Chemistry; Vol. 26, No. 3 (2014), 719-724

ASIAN JOURNAL OF CHEMISTRY

http://dx.doi.org/10.14233/ajchem.2014.15490

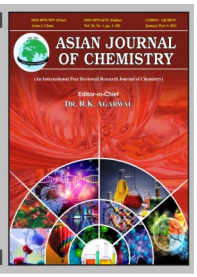

Nanosheet-Assembled Hematite Spheres for Adsorption of Cr(VI)

WEIWEI WANG* and JIALIANG YAO

School of Materials Science and Engineering, Shandong University of Technology, 12 Zhang Zhou Road, Zibo 255091, Shandong, P.R. China

*Corresponding author: Fax: +86 533 2781660; Tel: +86 533 2782198; E-mail: weiweiwangsd@aliyun.com

Received: 15 March 2013; *Accepted*: 24 July 2013; *Published online*: 30 January 2014; AJC-14621

Fabricating complex architectures with small building blocks is an effective method to increase its surface area and improve its performance in removal of heavy metal. However, the techniques for preparing iron oxide complex structures still remain a challenge because of the rapid hydrolysis of Fe(III). We prepared α-Fe_2O_3 hierarchical spheres with nanosheet building units by using ascorbic acid to control the concentration and speed of hydrolysis of Fe(III). The phase, morphology and size of samples were characterized by X-ray powder diffraction and scanning electron microscopy. Experimental results showed that ascorbic acid had an important effect on the morphology and size of samples. Their adsorption activities were determined using Cr(VI) present in aqueous solution. The adsorption process fitted to Freundlich isotherm models for α-Fe_2O_3 hierarchical spheres. The adsorption kinetics followed pseudo-second-order rate kinetic model and α-Fe_2O_3 hierarchical spheres exhibited a better Cr(VI) adsorption property.

Keywords: Hematite, Hierarchical sphere, Adsorption property, Cr(VI), Adsorption.

INTRODUCTION

Iron oxides (oxyhydroxides) (including α-Fe_2O_3 and FeOOH) represent inexpensive, abundant and stable materials for removal of heavy metal ions and solar energy conversion applications[1-3]. Among them, hematite (α-Fe_2O_3) is the thermal stable phase of iron oxides. It has been reported that α-Fe_2O_3 was a suitable adsorbent over natural pH (pH 6-9) at high arsenic concentrations[4,5]. α-Fe_2O_3 could also adsorb surfactants (SDS, Imbentin AGS/35, Triton X-100 and DDAB) from water with a much lower amount of powder[6]. Generally, the adsorption capacities are related to surface area[7,8]. A useful way to increase the surface area is to prepare nanosize materials. However, due to their small size, they are difficult to be separated from the treated solution[6]. There are still great demands on the synthesis of materials with high surface area and large size for the application as adsorbents. Fabricating well defined superstructures or complex architectures with small building blocks is a smart method to improve its performance in removal of heavy metal ions and electrochemical activity compared with conventional adsorbents[9]. For example, α-FeOOH microspheres composed by needles showed a fast adsorption rate for As(V) and Pb(II) in water[10]. Amorphous Fe_2O_3/γ-Fe_2O_3 core-shell nanostructures showed a strong adsorption capability for As(V)[11].

To fabricate these complex architectures, building blocks need enough time to grow or move to form these structures. α-Fe_2O_3 complex structures are relatively hard to synthesize, owing to the rapid hydrolysis rate of Fe(III) in aqueous solution. To circumvent these problems, hierarchical precursors were prepared first by using different additives to control the hydrolysis rate of Fe (III). α-FeOOH microspheres composed of needles were prepared by using ethylene glycol to control the reaction rate or the adsorption of glucose[10,12]. Cao *et al.* reported the preparation of dendritic α-Fe_2O_3 micropines using the weak dissociation of $K_3[Fe(CN)_6]$ under hydrothermal conditions[13]. Murugananandham *et al.*[14] prepared α-Fe_2O_3 micromaterials with wormlike porous by the formation of ferric oxalate complex. Tan *et al.*[15] found that ascorbic acid could selectively absorb on the (001) plane of γ-In_2Se_3 and resulted in the formation of γ-In_2Se_3 microspheres assembled by nanosheets. By using the reducing ability of ascorbic acid and the planar structure and the bond angle of carbonate ions, Liu *et al.* prepared $FeCO_3$ lamellar structure[16]. In our experiments, we used the chelate complex formed between ascorbic acid and Fe^{3+} to control the reaction rate. α-Fe_2O_3 hierarchical spheres composed of nanosheets were obtained by topotactic phase change. The α-Fe_2O_3 hierarchical spheres were used as adsorbent for removal of heavy metal ions present in water and showed a strong Cr(VI) ions removal capacity. The existence of a large number of pores in the α-Fe_2O_3 structures was extremely important for the improvement of adsorption ability. The large size of α-Fe_2O_3 hierarchical spheres made it easier to separate from water.

EXPERIMENTAL

Ferric chloride, ascorbic acid, sodium carbonate, ethanol and potassium dichromate were purchased from Sinopharm Chemical Reagent Co. Ltd. and used as received without further purification.

General procedure: Sample 1: $FeCl_3 \cdot 6H_2O$ (0.067 M), Na_2CO_3 (0.200 M) and ascorbic acid (0.075 M) were added to 40 mL of deionized water to form a solution (dark black). The solution was transferred into a 50 mL autoclave and maintained at 180 °C for 10 h. After cooled down to room temperature, the product was separated by centrifugation, washed with absolute ethanol and vacuum-dried at 50 °C for 4 h. In order to investigate the influence of hydrothermal treating time, we also prepared samples at different times (0.5, 1.5, 3, 5, 8 h). These samples were labeled as S1-0.5, S1-1.5, S1-3, S1-5, S1-8, respectively. Sample 2 was obtained under the same experimental conditions as sample 1 except without using ascorbic acid. The samples obtained at different times (0.5, 5h) were labeled as S2-0.5 and S2-5. For the preparation of α-Fe_2O_3, sample 1 and sample 2 was heated at 250 and 500 °C in air for 2 h, respectively. The samples were labeled as S1-T250, S1-T500, S2-T250, S2-T500.

Adsorption experiments of Cr(VI): Potassium dichromate was vacuum-dried at 120 °C for 2 h. Then $K_2Cr_2O_7$ was dissolved in deionized water to form stock solution. In the kinetics study of Cr(VI) adsorption, the initial Cr(VI) concentration was 1.2 mg/L. Reaction suspensions were prepared by adding samples (0.44 g/L) to 250 mL of Cr(VI) stock solution. Analytical samples were drawn from the suspension by centrifugation and analyzed by ICP-AES. For the equilibrium adsorption isotherm study, samples with a loading of 0.5 g/L were added to 25 mL of Cr(VI) stock solutions with different initial concentrations (5, 15, 25, 50, 100, 200 and 400 mg/L). These solutions were stirred at room temperature for 24 h. The Cr(VI) concentration in the remaining solution was measured by ICP-AES. The amount of Cr(VI) adsorbed at equilibrium (q_e, mg/g) was calculated from formula: $q_e = (C_0-C_e)V/m$, where C_0 and C_e represent the concentration of Cr(VI) before and after removal process, respectively. V is the solution volume and m is the weight of the adsorbent.

Detection method: X-ray powder diffraction (XRD) patterns were recorded using a D8 ADVANCE X-ray diffractometer with high-intensity CuK_α radiation ($\lambda = 1.5406$ Å). Scanning electron microscopy (SEM) micrographs were recorded on a FEI-Sirion 200 field emission scanning electron microscope. Thermogravimetric analysis (TG) and differential thermal analysis (DTA) were carried out on a NETZSCH STA 449 C thermal analyzer with a heating rate of 10 °C/min in air. The concentration of Cr(VI)was analyzed on an induced coupled plasma atomic emission spectrometer (PE Optima 2100DV ICP-AES). Fourier transform infrared (FTIR) spectroscopy was obtained on a Thermo Nicolet 5700.

RESULTS AND DISCUSSION

XRD and FTIR analysis were used to confirm the composition of samples. After adding ascorbic acid, sample 1 was amorphous and no distinct diffraction peaks for iron oxide were observed (Fig. 1a). The bands at 798 and 531 cm^{-1} (Fig. 1c, sample 1) could be assigned to the stretching mode of α-FeOOH[17]. Fig. 2a showed the absorbance spectrum of sample 1. According to the secondary derivative of Fig. 2b, the band at 1676 cm^{-1} was composed of four peaks (at 1715, 1683, 1621 and 1560 cm^{-1}, Fig. 1e). The bands centered at 1715, 1683 and 1067 cm^{-1} could be assigned to the C=O, C=C and C-O-C stretching vibrations of ascorbic acid, respectively[15,18]. So sample 1 was amorphous α-FeOOH adsorbed with ascorbic acid. Sample 1 was spheres composed of many nanosheets. The thickness of nanosheets was about 50 nm (Fig. 3a and 3b). Without using ascorbic acid, sample 2 showed some weak diffraction peaks and could be assigned to the hexagonal α-Fe_2O_3 phase (Fig. 1b, JCPDS file No. 89-0599). Two bands at 568 cm^{-1} and 482 cm^{-1} were clearly visible, which could be assigned to α-Fe_2O_3 phase (Fig. 1d)[19]. This also confirmed the formation of α-Fe_2O_3. Sample 2 was nanoparticles with size of 50 nm (Fig. 3c). Ascorbic acid affected both the phase and the morphology of samples.

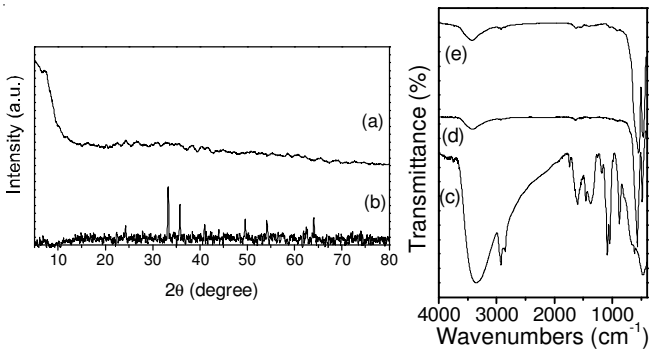

Fig. 1. XRD patterns of (a) sample 1, (b) sample 2, FTIR spectra of (c) sample 1, (d) sample 2, (e) S1-T500

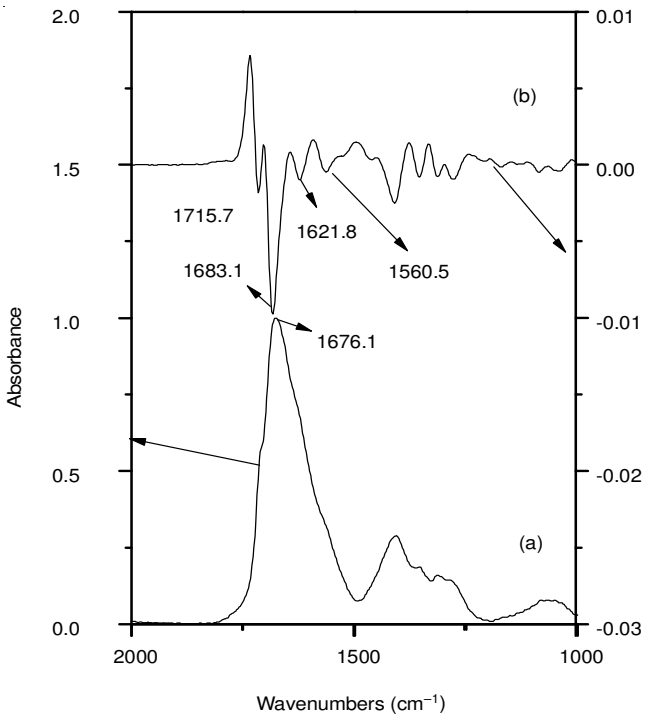

Fig. 2. FTIR spectra (a) the absorbance spectrum of sample 1, (b) secondary derivative FTIR of sample 1

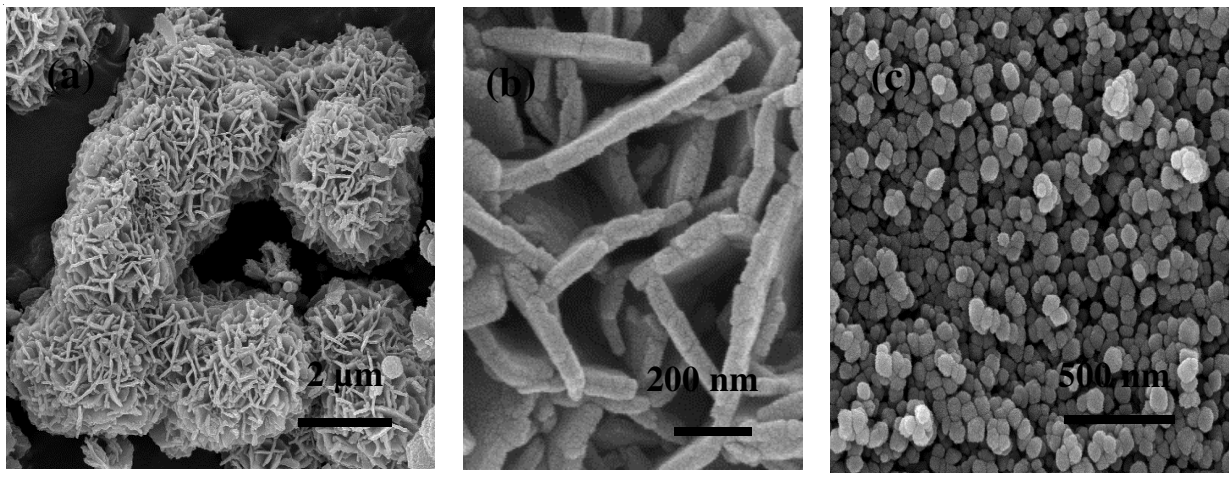

Fig. 3. SEM images of (a) and (b) sample 1, (c) sample 2

The thermal behaviours were also investigated and chose the decomposition temperature by TG/DTA analysis (Fig. 4). There were two exothermic peaks in DTA for sample 1 (Fig. 4a, 255.1 °C and 339.3 °C). The corresponding weight loss was measured to be 61 % and nearly completed by 360 °C. Further increasing the temperature, no distinct weight loss was observed. The final product was confirmed to be α-Fe_2O_3 by XRD (S1-T500, Fig. 5c). However, the DTA curve for sample 2 showed a broad exothermal peak at 309.3 °C (Fig. 4b). The corresponding weight loss was measured to be 3 % and completed by 450 °C. According to the above XRD/FTIR analysis, the large weight loss for sample 1 was due to the decomposition of the adsorption ascorbic acid and α-FeOOH. We chose 500 °C as the decomposition temperature of sample 1. This was confirmed by identifying the phase formed at different temperatures by FTIR and XRD studies (Fig. 1 and 5).

When sample 1 was heated in air at 250 °C for 2 h, S1-T250 with poor crystallinity (Fig. 5a), consistent with the analysis of TG/DTA (Fig. 4a). When sample 2 was heated under the same conditions as that of S1-T250, S2-T250 showed several weak diffraction peaks for α-Fe_2O_3 (JCPDS File No. 89-0599, Fig. 5b). As the calcination temperature increased to 500 °C, both samples were in red color and well-crystallized hexagonal α-Fe_2O_3 was obtained (S1-T500 and S2-T500, Figs. 5c and 5d). Compared with that of S1-T500, the crystallinity of S2-T500 improved. The shape and size of all samples did not change distinctly after calcination (Fig. 6). After calcined at 500 °C, S1-T500 was spheres composed of nanosheets (Fig. 6a). From the standing nanosheets in Fig. 6b, the thickness of α-Fe_2O_3 nanosheets was less than 50 nm. The thickness of nanosheets decreased slightly after calcined. S2-T500 was nanoparticles. The size of S2-T500 was increased compared with that of sample 2 (Figs. 6c and 6d). We noted that the XRD results were in agreement with FTIR measurements (Fig. 5). After calcination at 500 °C (S1-T500, Fig. 1e), the bands between 2000-1000 cm^{-1}, which were attributed to the absorbed ascorbic acid, disappeared. Two new bands at 548 cm^{-1} and 467 cm^{-1} were clearly visible, which could be assigned to α-Fe_2O_3 phase[19]. But it is shifted to lower wavenumber compared with that of sample 2. It has been reported that the shape, size and crystallization of α-Fe_2O_3 particles influenced the corresponding FTIR spectrum[12,19]. S1-T500 was α-Fe_2O_3 microspheres composed of sheets and sample 2 was α-Fe_2O_3 particles. The difference in structures and shapes between them resulted in the shift of peaks.

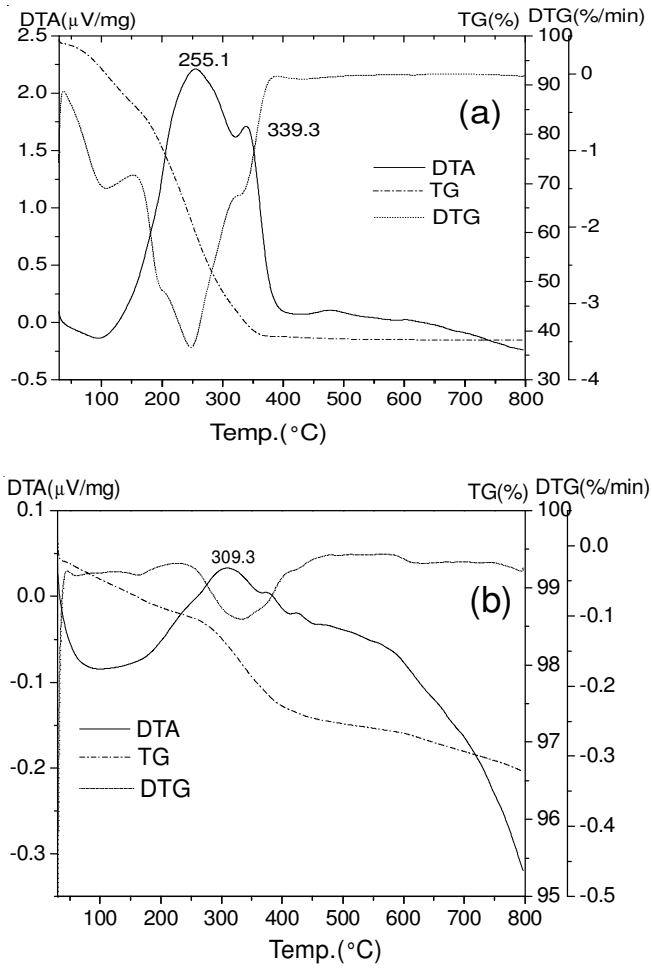

Fig. 4. TG/DTG/DTA curves of (a) sample 1, (b) sample 2

Based on the SEM/XRD studies of samples, we found that ascorbic acid played a crucial role in the formation of α-Fe_2O_3 hierarchical spheres. It has been reported that α-Fe_2O_3 microspheres were prepared in the presence of ascorbic acid[16]. They found that Fe^{3+} was reduced by ascorbic acid and $FeCO_3$ was obtained. The formation of $FeCO_3$ lamellar structure was due to the planar structure and the bond angle of carbonate

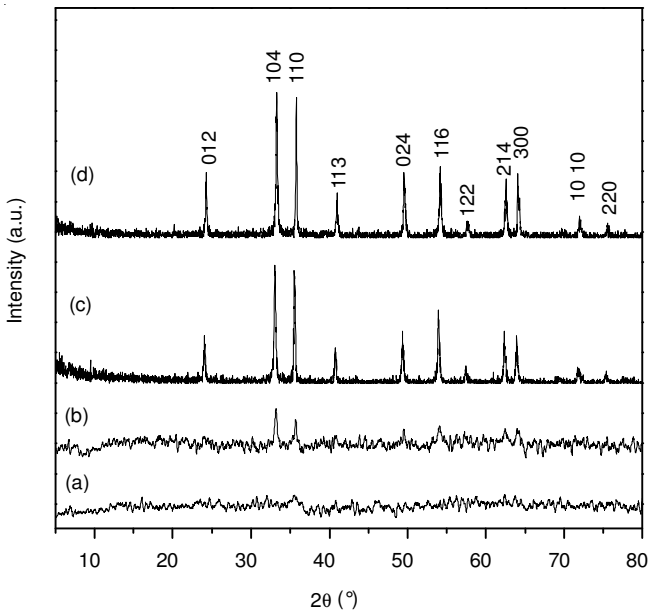

Fig. 5 XRD patterns of (a) S1-T250, (b) S2-T250, (c) S1-T500, (d) S2T500.

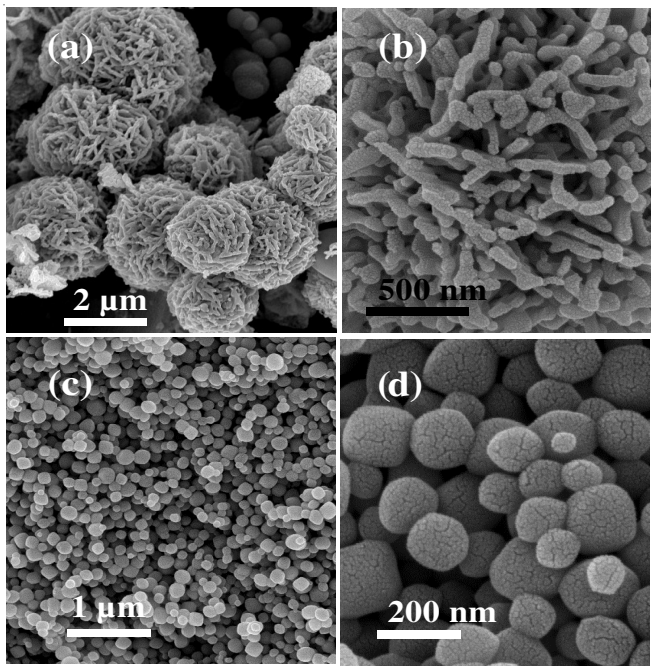

Fig. 6. SEM images of (a) and (b) S1-T500, (c) and (d) S2-T500

ions. Although using ascorbic acid, we found the formation of α-Fe_2O_3 hierarchical spheres in our experiments followed the different mechanism. No $FeCO_3$ was observed and amorphous α-FeOOH formed. Ascorbic acid could reduce Fe^{3+} in aqueous solutions below pH 6.2, but above pH 6.8, ascorbic acid was not an effective reducing agent for Fe^{3+} [20]. Ascorbic acid could form soluble chelate complex with Fe^{3+} [21]. The chelate complex was unstable and decomposed with increasing temperature, which could gradually release Fe^{3+} and retard the hydrolysis rate of Fe^{3+} during the hydrothermal process[22]. In present experiments, the pH value of solution was about 8.2 with ascorbic acid. No precipitation appeared at room temperature and only uniform solution was obtained. After hydrothermal reaction for 0.5 h (S1-0.5), irregular particles appeared (Fig. 7a). From the magnified image (Fig. 7b), we could see that the boundary between particles was unobvious. And it seemed that many particles grew from one point (indicated as an arrow in Fig. 7b). Upon prolonging the reaction time to 1.5 h, the size of particles increased and some irregular sheets appeared near the particles (S1-1.5, indicated as an arrow in

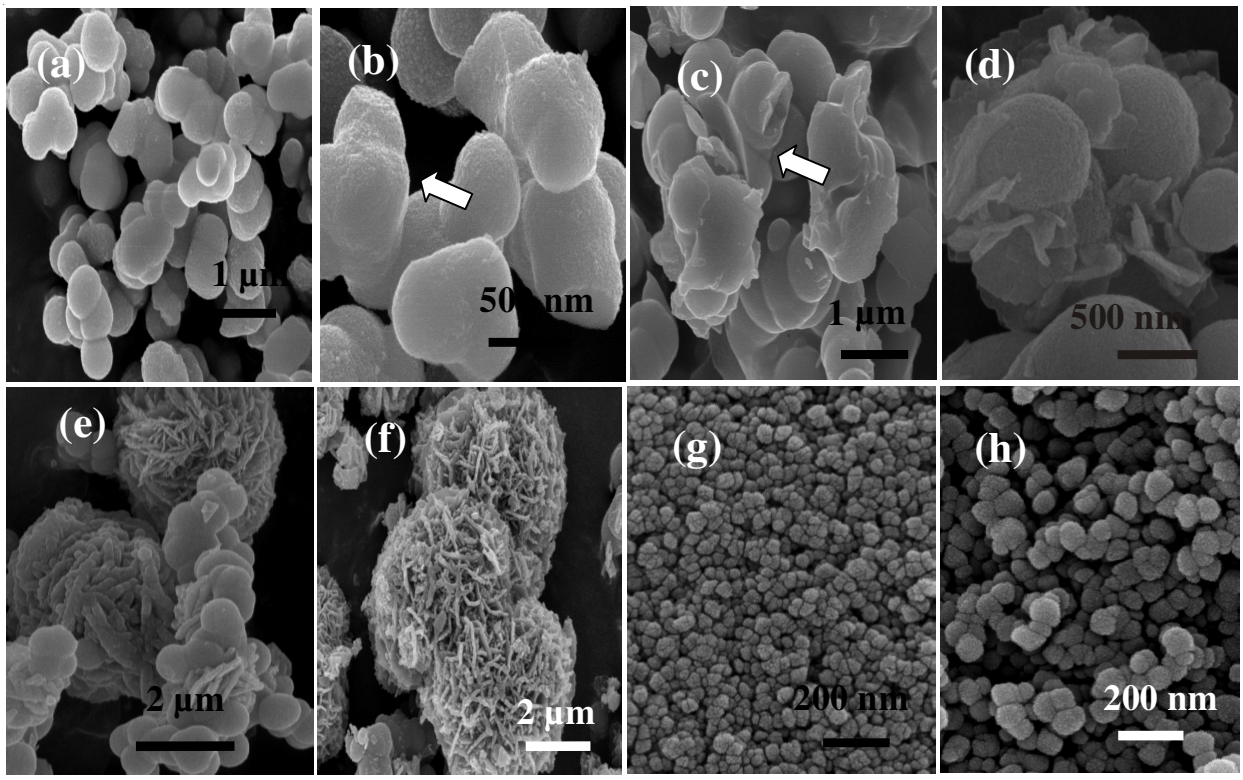

Fig. 7. SEM images of (a) and (b) S1-0.5, (c) S1-1.5, (d) S1-3, (e) S1-5, (f) S1-8, (g) S2-0.5, and (h) S2-5

Fig. 7c). In general, small particles dissolve easier than large particles. After the small particles dissolved, some ions released and recrystallized. The presence of un-dissolved particles could lower the nucleation energy and secondary nucleation occurred around the un-dissolved particles, followed by the branched structures[23,24]. The slow supply of ions caused a relatively low Fe^{3+} concentration in the solution, which promoted 2D growth and favored the generation of nanosheets [25,26]. Then the nano-units surrounding nuclei grew in the form of sheets and hierarchical spheres composed of nanosheets were formed. It could be confirmed by SEM results that the particles were wrapped by sheets and then the amount of particles decreased and lots of spheres composed of nanosheets appeared with longer reaction time (S1-3, S1-5, S1-8, Figs. 7d-7f). After calcined, it transformed into α-Fe_2O_3 with the similar morphology.

Without ascorbic acid, red color precipitation was obtained at room temperature. The presence of CO_3^{2-} caused the quick formation of $Fe(OH)_3$ by the reaction between Fe^{3+} and CO_3^{2-} (function 1). The hydrothermal reaction resulted in the decomposition of $Fe(OH)_3$ to form α-Fe_2O_3 (function 2). After hydrothermal reaction for 0.5 h, particles with size of 50 nm were obtained (S2-0.5, Fig. 7g). Upon prolonging the reaction time to 5 h (S2-5), the phase was the same as that of S2-0.5, but the size of the particles increased (Fig. 7h).

$$2Fe^{3+} + 3CO_3^{2-} + 3H_2O \rightarrow 2Fe(OH)_3 + 3CO_2\uparrow \quad (1)$$

$$2Fe(OH)_3 \rightarrow \alpha - Fe_2O_3 + 3H_2O \quad (2)$$

According to the speciation diagram of Cr(VI), the major form was $HCrO_4^-$ at pH below 4 while CrO_4^{2-} at pH above 9. Increasing pH from 6 to10, the molar fraction of the $HCrO_4^-$ was diminished from 77 % to 0.003 %[27]. In our experiments, the pH value was about 7.5 for the adsorption experiments. The predominant Cr(VI) species were CrO_4^{2-} and Cr(VI) was mainly adsorbed as CrO_4^{2-}. The kinetics of Cr(VI) adsorption onto α-Fe_2O_3 hierarchical spheres (S1-T500) and particles (S2-T500) were shown in Fig. 8. The adsorption of Cr(VI) was rapid at first and then slowed (Fig. 8a). In our experimental conditions, most of Cr(VI) could be removed after 3 h. The adsorption kinetic experimental data could be best fitted into a pseudo-second-order rate kinetic model: $t/q_t = 1/k_2q^2_e + t/q_e$. Where k_2 is the rate constant of the pseudo-second-order model of adsorption [g/(mg min)], q_t is the amount of Cr(VI) adsorbed at time t and q_e is the equilibrium adsorption capacity. The values of k_2 and q_e were obtained by a plot of t/q_t against t (Fig. 8b and Table-1), which showed that the pseudo-second-order model best represented the adsorption kinetics in our adsorbent systems. The value of calculated q_e was very close to that of experimental q_e.

TABLE -1
KINETICS PARAMETERS OF Cr(VI) ADSORPTION ONTO SAMPLES

Sample No.	K_2 (g/(mg min))	q_e (mg/g)	R^2	Experimental q_e (mg/g)
S1-T500	0.1896	0.7347	0.9996	0.7248
S2-T500	0.0677	0.6660	0.9967	0.6421

To evaluate the Cr(VI) adsorption capacity of samples, the adsorption isotherm was conducted, as shown by the dots in Figs. 8c and 8d. It could be seen that the amount of Cr(VI) adsorbed at equilibrium (q_e) was increased with the increasing of C_e. The Langmuir adsorption model $q_e = q_m bC_e/(1 + bC_e)$ and Freundlich adsorption model $\ln q_e = \ln C_e/n + \ln K_F$ were used to calculate the maximal adsorption capacity, where q_m (mg g^{-1}) is the maximal adsorption capacity. The experimental data fitted well to the Freundlich adsorption model rather than the Langmuir adsorption model. The regression coefficient (R^2) for the Freundlich adsorption model was 0.97, higher than that of Langmuir adsorption model (0.96). This suggested that the Cr(VI) adsorption behavior could be regarded as a multi-layer adsorption process. Compared with that of S2-T500, α-Fe_2O_3 hierarchical spheres (S1-T500) showed better adsorption ability. The maximal Cr(VI) removal capacity (q_m) for S1-T500 was 148.5714 mg/g while 30.0875 mg/g for S2-T500 within our experimental range. The maximal Cr(VI) removal capacity (q_m) for S1-T500 was much higher than those reported for the Cr(VI) removal[28-30]. Table-2 showed that α-Fe_2O_3 nanoparticles exhibited a lower q_m than α-Fe_2O_3 microspheres. Compared with S2-T500, S1-T500 showed higher diffusion rate and more adsorption amount. It was due to the structure of S1-T500. For S1-T500, Cr(VI) was initially adsorbed on the exterior surface of the microspheres. When the adsorption at the exterior surface reached the saturation level, Cr(VI) began to move into the interior of microspheres. When Cr(VI) diffused into the interior of microspheres, the diffusion resistance was increased, which in turn led to a decrease in diffusion rate. Fabricating α-Fe_2O_3 hierarchical spheres composed of nanosheets was demonstrated to be an effective method to improve their adsorption properties.

TABLE-2
EQUILIBRIUM ADSORPTION ISOTHERMS FITTING PARAMETERS FOR Cr(VI)

Sample No.	Langmuir			Freundlich		
	q_e (mg/g)	b	R^2	n	K_F	R^2
S1-T500	148.5714	0.0123	0.9601	1.6693	5.2059	0.9747
S2-T500	30.0875	0.0101	0.9677	1.6497	1.0932	0.9712

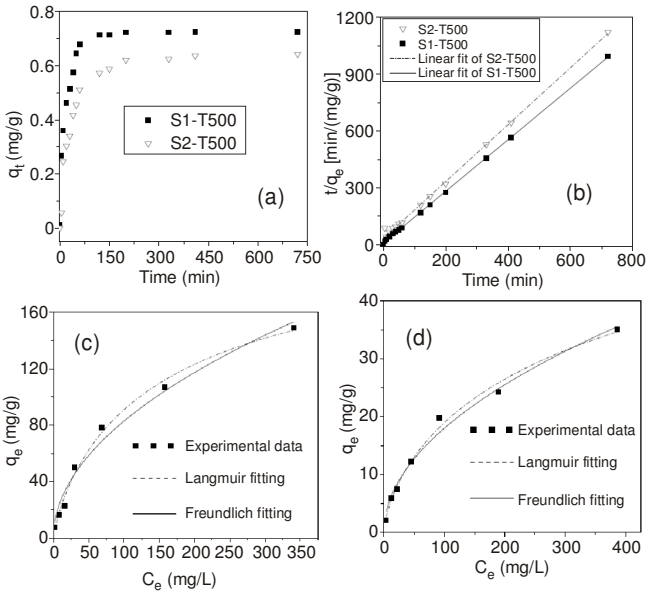

Fig. 8. (a) Effects of contact time on the adsorption of Cr(VI), (b) pseudo-second-order kinetic plots for the adsorption of Cr(VI). Adsorption isotherms of Cr(VI) using (c) S1-T500 and (d) S2-T500

Conclusion

α-Fe_2O_3 hierarchical spheres composed of nanosheets were synthesized *via* a hydrothermal synthesis method, based on controlling the concentration and hydrolysis rate of iron ions. The soluble chelate complexes between ascorbic acid and Fe(III) reduced the hydrolysis rate and concentration of Fe(III), which favored the formation of hierarchical spheres composed of nanosheets. Without ascorbic acid, only α-Fe_2O_3 nanoparticles were obtained. The obtained α-Fe_2O_3 had abundant holes and large size and thus possessed high surface areas and dramatically improved Cr(VI) adsorption performance.

ACKNOWLEDGEMENTS

Financial supports from Shandong Provincial Natural Science Foundation of China (No. ZR2010EM059), Shandong Education Department of International Cooperation Training Program (No. 2007:207091) and Development of Young Teachers Program of Shandong University of Technology (No. 4072:110019) are acknowledged.

REFERENCES

1. Y. Yang, H.X. Ma, J. Zhuang and X. Wang, *Inorg. Chem*., **50**, 10143 (2011).
2. C. Baumanis, J.Z. Bloh, R. Dillert and D.W. Bahnemann, *J. Phys. Chem. C*, **115,** 25442 (2011).
3. X.W. Song and J.F.O. Boily, *J. Phys. Chem. C*, **115**, 17036 (2011).
4. Y. Mamindy-Pajany, C. Hurel, N. Marmier and M. Roméo, *Desalination*, **281**, 93 (2011).
5. Y. Mamindy-Pajany, C. Hurel, N. Marmier and M. Roméo, *C. R. Chimie,* **12**, 876 (2009).
6. C.C. Borghi, M. Fabbri, M. Fiorini, M. Mancini and P.L. Ribani, *Sep. Purif. Technol*., **83**, 180 (2011).
7. T.J. Reich and C.M. Koretsky, *Geochim. Cosmochim. Acta* **75**, 7006 (2011).
8. R.M. Tinnacher, M. Zavarin, B.A. Powell and A.B. Kersting, *Geochim. Cosmochim. Acta*, **75**, 6584 (2011).
9. Z. Sun, J.H. Kim, Y. Zhao, F. Bijarbooneh, V. Malgras, Y. Lee, Y.M. Kang and S.X. Dou, *J. Am. Chem. Soc*., **133**, 19314 (2011).
10. H. Li, W. Li, Y.J. Zhang, T.S. Wang, B. Wang, W. Xu, L. Jiang, W.G. Song, C.Y. Shu and C.R. Wang, *J. Mater. Chem*., **21**, 7878 (2011).
11. F.Z. Mou, J.G. Guan, Z.D. Xiao, Z.G. Sun, W.D. Shi and X. Fan, *J. Mater. Chem*., **21**, 5414 (2011).
12. G.X. Tong, J.G. Guan and Q.J. Zhang, *Mater. Chem. Phys*., **127**, 371 (2011).
13. G. Sun, B.X. Dong, M.H. Cao, B.Q. Wei and C.W. Hu, *Chem. Mater*., **23**, 1587 (2011).
14. R. Amutha, M. Muruganandham, M. Sathish, S. Akilandeswari, R.P.S. Suri, E. Repo and M. Sillanpaa, *J. Phys. Chem. C*, **115**, 6367 (2011).
15. X.Y. Tan, J. Zhou and Q. Yang, *CrystEngComm*, **13**, 2792 (2011).
16. G. Liu, Q. Deng, H.Q. Wang, D. H. L. Ng, M. Kong, W.P. Cai and G.Z. Wang, *J. Mater. Chem*., **22**, 9704 (2012).
17. S. Krehula, S. Music, Z. Skoko and S. Popovic, *J. Alloys Comp*., **420**, 260 (2006).
18. C.Y. Panicker, H.T. Varghese and D. Philip, *Spectrochim. Acta A*, **65**, 802 (2006).
19. M. Zic, M. Ristic and S. Music, *J. Alloys Compd*., **464**, 81 (2008).
20. Y.H.P. Hsieh and Y.P. Hsieh, *J. Agric. Food Chem*., **48**, 1569 (2000).
21. V. Kuellmer, Ascorbic Acid, Kirk-othmer Encyclopedia of Chemical Technology, John Wiley & Sons, New York, edn. 5 (2007).
22. G.F.M. Ball, Vitamins: Their Role in the Human Bod, Wiley-Blackwell, Oxford, edn 1 (2004).
23. G. Xi, Y. Peng and W. Yu and Y. Qian, *Cryst. Growth Des*., **5**, 325 (2005).
24. G. Xi, K. Xiong, Q. Zhao, R. Zhang, H. Zhang and Y. Qian, *Cryst. Growth Des*., **6**, 577 (2006).
25. H. Zhou and Z. Li, *Mater. Chem. Phys.,* **89**, 326 (2005).
26. S.A. Morin, A. Forticaux, M.J. Bierman and S. Jin, *Nano Lett*., **11**, 4449 (2011).
27. I.H. Yoon, S. Bang, J. S. Chang, M. G. Kim and K.W. Kim, *J. Hazard. Mater*., **186**, 855 (2011).
28. W. Kuang, Y. Tan and L. Fu, *Desalin. Water Treat*., **45**, 222 (2012).
29. G. Cheng, J. Xiong, H. Yang, Z. Lu and R. Chen, *Mater. Lett*., **77,** 25 (2012).
30. Z. Wu, S. Li, J. Wan and Y. Wang, *J. Mol. Liq*., **170**, 25 (2012).